Page 1 of 12. Royal Aeronautical Society 2018

Numerical Study of Incipient Transonic Shock Buffet on Large Civil Aircraft Wings

Panagiotis Belesiotis-Kataras
p.belesiotis-kataras@liverpool.ac.uk
PhD Student
School of Engineering
University of Liverpool
United Kingdom

Sebastian Timme
sebastian.timme@liverpool.ac.uk
Senior Lecturer
School of Engineering
University of Liverpool
United Kingdom

ABSTRACT

Shock buffet, a self-sustained flow unsteadiness found on the wings of large civil aircraft in high-speed edge-of-the-envelope flight even in the absence of structural vibration, remains an interesting topic within transonic aerodynamics. Its elucidation would benefit the more efficient design of the wings of the future. In this study we investigate how changes in the design philosophy of two such aircraft wings, with their conception separated by decades, have impacted the characteristics of the instability in the vicinity of the respective design Mach numbers and onset angles of attack. We adopt the toolset of time-linearised Reynolds-averaged Navier–Stokes aerodynamics within an industrial computational fluid dynamics package to discuss both forced harmonic structural excitation and global stability analysis on the rigid wing. It is demonstrated that, despite distinct differences in the underlying base flows for the two wings e.g. in terms of reverse-flow regions, the dynamic responses of both integrated and distributed loads show intriguing similarities. While no universal shock buffet model for wings is proposed herein, the results suggest that it might exist.

1.0 INTRODUCTION

Designing next generation aircraft wings requires a firm understanding of unsteady aerodynamic loads, given the flight conditions, at all times. The ever increasing needs of modern air transport require safer aircraft that have a reduced environmental impact. To meet these requirements, the phenomena encountered in high-speed transonic flight conditions, which make up the majority of the total cruising flight time, are critical to be studied. Shock buffet, as one of those, is a transonic flow instability emerging from the interaction of shock waves and separated boundary layers producing self-sustained shock wave oscillations, mainly observed on supercritical wings in high-speed edge-of-the-envelope flow conditions. The appearance of unsteady shock-induced separated flow comes with a drag penalty, and transient loads can excite the wing structure (called buffeting) resulting in an increase in fuel consumption and emissions, poorer flight performance and a general degrading of the handling qualities of the aircraft. To date, this phenomenon is mitigated by limiting the flight envelope of the aircraft, allowing a 30% margin from the cruise point to buffet onset during the design process[1]. Consequently, the phenomenon of shock buffet has gained significant research interest since its discovery over six decades ago[2].

Initial studies of shock buffet on aerofoils focussed on establishing a better understanding of the underlying dynamic mechanisms of the instability as well as to create models that can accurately describe the shock-wave motion and predict the instability onset. Lee's[3] wave-propagation feedback model was able to describe the self-sustained shock-wave oscillations, while the global stability approach of Crouch et al.[4,5] showed that the onset of the aerofoil instability occurs when an eigenvalue crosses the imaginary axis into the unstable half-plane, establishing a Hopf bifurcation. Different experimental studies supported both descriptions, when similar oscillation frequencies (i.e. Strouhal numbers in the range of 0.05 to 0.08) were observed in wind tunnel tests, and also demonstrated that the governing physics of the phenomenon on aerofoils is mainly two-dimensional[6,7].

Conversely, wind tunnel tests on transport-type swept wings showed the first discrepancies between the behaviour of two- and three-dimensional shock buffet, with the latter case demonstrating oscillation frequencies up to an order of magnitude higher than its two-dimensional counterpart with Strouhal numbers (based on mean aerodynamic chord) ranging from 0.2 to 0.7[8]. For the three-dimensional case, more severe unsteadiness was observed close to the wing tip[9]. Complementary numerical studies revealed that these differences result from wing sweep[10], with three-dimensional effects becoming dominant for sweep angles of 20° and above. It is worth pointing out here that modern large aircraft wings have a typical sweep angle of about 30°. In addition, an increasingly broadband frequency spectrum is observed when moving beyond the onset conditions for the three-dimensional case, in contrast to the distinct frequency of two-dimensional buffet, even beyond the instability onset.

Different strategies have been pursued in the past to predict the onset of shock buffet instability with the most common buffet indicators looking at the structural response of the wing, breaks in the slopes of integrated aerodynamic coefficients or trailing-edge pressure divergence[11]. For aircraft in flight, acceleration at the pilot seat is measured in the certification stage to ensure that buffeting conditions remain outside the flight envelope[1]. Experimental analyses of these indicators show that

there are distinct responses of the phenomenon depending on the angle of attack. In particular, the flow remains steady for small incidence angles, while it demonstrates small amplitude shock oscillations with a narrow bump in the pressure spectra at Strouhal numbers of about 0.3 for moderate incidence [12]. Large amplitude aperiodic oscillations with broadband spectra are observed for high incidence [13].

On the numerical side, industry-standard Reynolds-averaged Navier–Stokes (RANS) simulations have resulted in good agreement with experimental data and, in the case of unsteady RANS and detached-eddy simulation, the shock motions, including mean values and standard deviation, have successfully been reproduced [14,15,16]. Further numerical studies, using forced harmonic structural excitation, have demonstrated that small increments in incidence around the onset angle of attack result in two distinct responses of the integrated aerodynamic coefficients, specifically a lower-frequency peak for Strouhal numbers around 0.1 and a higher-frequency behaviour in the Strouhal number range between 0.2 and 0.7, that is amplified when shock buffet is imminent. While pseudo-resonance due to the non-normality of the Navier–Stokes equations (or a convective instability) could explain the lower-frequency behaviour, the higher-frequency response supports the existence of an absolute instability. This is also emphasised by stability analyses in the pre-buffet regime that show eigenvalues migrating towards the unstable region when approaching the onset angle of attack, hinting that the origin of the instability is due to a Hopf bifurcation [17]. Indeed, recent investigations for the origin of the instability of three-dimensional shock buffet have suggested that the onset is related to an unstable global mode [18], an observation previously discussed for the two-dimensional aerofoil case [4], with its spatial structure describing the so-called buffet cells propagating outboard in the span-wise direction.

In the present paper, unsteady RANS simulations on two large civil aircraft wings, specifically an older 1970s design referred to as RBC12 and the more recent NASA Common Research Model, are analysed using methods of linearised frequency-domain aerodynamics. For both wing geometries the structure is excited for a range of frequencies using a synthetic structural torsion mode at different angles of attack. In addition, we present some results of a three-dimensional global stability study. The comparison of various flow indicators shows how changes in the wing design philosophies have affected the dynamic phenomenon of shock buffet, specifically its onset.

2.0 NUMERICAL SETUP

RBC12 Model

The RBC12 model is a half wing-body configuration scaled to wind tunnel dimensions. It has a quarter-chord sweep of 25°, a reference area of 0.296 m^2, an aerodynamic mean chord of 0.279 m, a semi-span of 1.104 m and an aspect ratio of 7.78 [11]. The wing is also twisted and tapered, as shown in Figure 1(a). The computational grid is composed of about 2.7 million points using an unstructured mesh produced using the Solar mesh generator and following industry accepted guidelines. The focus is on a Mach number of 0.8 and the Reynolds number (based on the aerodynamic mean chord) is 3.75 million. Far-field conditions are applied at a distance of 25 times the semi-span of the model and a symmetry boundary condition is applied along the centre plane. This wing geometry has been studied extensively by the authors in the past [15,16,17].

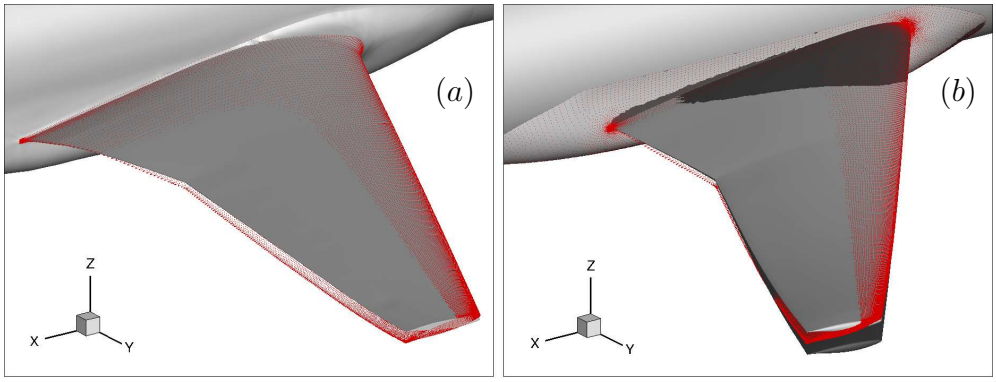

Figure 1: Illustration of wing deformation due to synthetic torsion mode for (a) RBC12 and (b) CRM. The CRM wing also shows a representative static deformation in comparison to the undeformed reference shape.

NASA Common Research Model

The NASA Common Research Model (CRM) is a half wing-body generic commercial aircraft configuration. The modern supercritical wing, shown in Figure 1(b), has a quarter-chord sweep angle of 35°, a reference area of 0.280 m^2, a taper ratio of 0.275, an aerodynamic mean chord of 0.189 m, a semi-span of 0.793 m and an aspect ratio of 9[19]. Specifically, we use the wing-body-tail configuration with 0° tail setting angle. The Mach number in the current study is 0.85 with a Reynolds number (based on the aerodynamic mean chord) of 5 million per reference chord. The computational mesh has about 6.2 million points, generated using the Solar mesh generator just like the RBC12, and the hemispherical far-field boundary is located at a distance of approximately 100 semi-spans from the body. Symmetry boundary condition is applied along the centre plane. In addition, depending on the angle of attack, unlike the RBC12, the static deformation of the wing, measured in the European Transonic Windtunnel campaign, is taken into account. This deformation, for a representative angle of attack, is also highlighted in Figure 1(b).

Steady-state and Linearised Flow Solver

The unstructured finite-volume solver TAU, developed by the German Aerospace Centre (DLR) and used both in industry and academia, was chosen for the simulations. Second-order spatial discretisation uses the standard central scheme with artificial dissipation. While scalar dissipation is used for the RBC12, matrix dissipation is selected for the CRM. Turbulence closure is achieved using the negative Spalart-Allmaras one-equation model, discretized with a first-order upwind scheme. The Green-Gauss theorem is used for reconstructing the gradients of the flow variables. An implicit backward Euler solver converges the non-linear flow equations to steady state. All steady solutions converged by at least ten orders of magnitude.

For the linearised frequency-domain analysis (and complementary eigenvalue computations), the RANS equations are first discretised in space and then linearised about

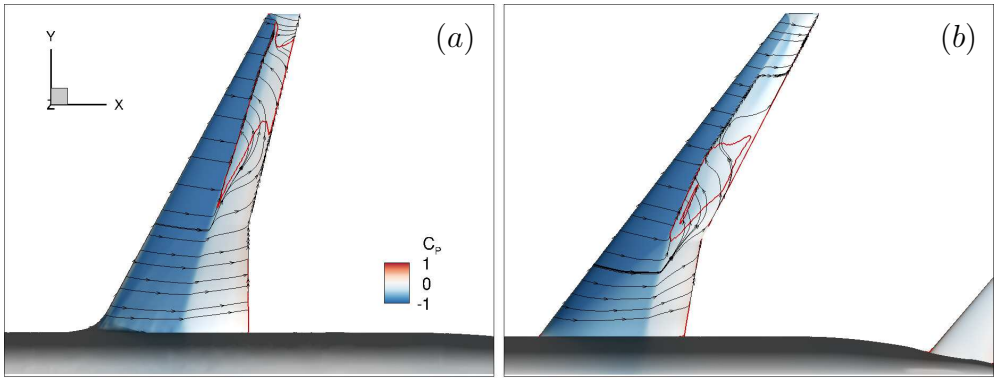

Figure 2: Steady-state surface pressure coefficient with friction lines for (a) RBC12 at $\alpha = 3°$ and (b) CRM at $\alpha = 3.7°$. The zero skin friction line is highlighted in red.

the steady-state base flow. Note that the turbulence model is fully coupled with the mean flow equations and linearised accordingly. A block incomplete lower-upper factorisation preconditions the chosen Krylov sparse iterative linear solver; specifically a generalized conjugate residual solver with deflated restarting is used[20]. The linearised flow solver has been scrutinised previously both for an aerofoil and a wing in such edge-of-the-envelope flow conditions[21]. In essence, our linearised aerodynamics analyses consider a small unsteady change $\widetilde{\boldsymbol{u}}$ in the flow field variables (including the unknowns of the turbulence model) with respect to a steady base flow $\bar{\boldsymbol{u}}$. The unsteady part is formed as a complex-valued amplitude function $\widehat{\boldsymbol{u}}$ in three-dimensional space times a time-dependent exponential function $e^{\lambda t}$, where t is the time and λ is either simple harmonic (i.e. $\lambda = i\omega$ with ω as angular frequency and i as the imaginary unit) for forced excitation or damped harmonic (i.e. $\lambda = \sigma + i\omega$ with σ as growth rate) for the eigenvalue computation. The implicitly restarted Arnoldi method[22], as implemented in the ARPACK library[23], is used for the latter calculations. The baseline linearised frequency-domain solver is adapted to solve linear systems arising from the shift-and-invert spectral transformation within the Arnoldi iterations[18].

The synthetic torsion modes for the two wings, used for the structural excitation of the system, are shown in Figure 1. A synthetic mode resembles a typical wing deformation (e.g. bending and/or torsion) but the mode itself is not based on a finite-element analysis of the actual wing structure. Specifically in this study, excitation follows a forced sinusoidal torsion deformation of the wing with the axis of rotation located approximately at the quarter-chord line. The deformation of the wing is zero at the root while increasing towards the wing tip.

3.0 RESULTS

The steady-state surface pressure distributions for both models with representative skin friction lines are shown in Figure 2. Values of zero skin friction are highlighted, too. At the chosen flow conditions, specifically angle of attack α, with buffet onset being imminent, the RBC12 has a lift coefficient (C_L) of 0.57, while the CRM has

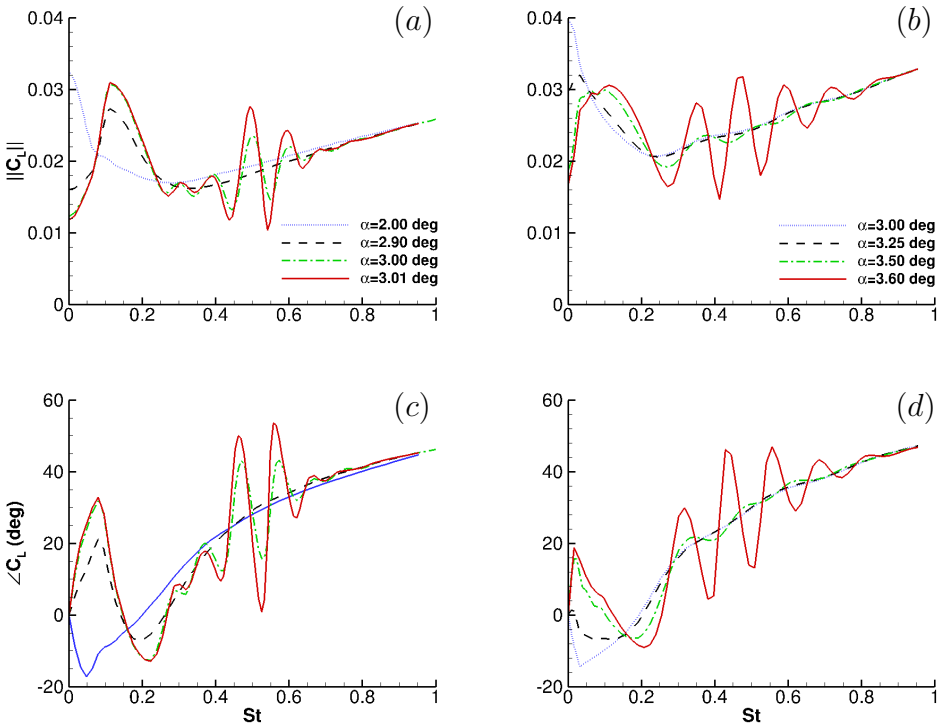

Figure 3: Frequency response of lift coefficient (C_L) showing magnitude and phase around buffet onset angle of attack for the RBC12 (a),(c) and CRM (b),(d).

about 0.60. Both models exhibit, as expected at the chosen conditions, a clear shock wave pattern. First differences between old and new wing designs can be observed with the RBC12 demonstrating a larger reverse-flow area downstream of the shock than that of the CRM. In addition, the separated area of the CRM is located closer to the crank compared with the RBC12 where it is closer to the wing tip. Such steady flow fields are used as the starting point for the time-linearised dynamic analyses.

Figure 3 presents the variation of the lift coefficient magnitude and phase for different angles of attack in pre-buffet conditions for a typical range of frequencies. As the incidence is increased, a first resonant peak appears for a Strouhal number St of about 0.1 that reaches its local maximum when approaching the onset angle of attack. In this low-frequency range, the aerodynamic response shows a phase lead over the structural excitation with increasing frequency until the peak in magnitude is reached. Similar response behaviour has been reported previously for aerofoils[24]. With buffet onset being imminent, incremental increases of the angle of attack result in a distinct behaviour on both wings at higher frequencies, as the structural excitation appears to excite the shock buffet dynamics. While the lower frequency peak remains mostly unaffected, a strong amplification is observed in the higher frequency range with Strouhal numbers of about 0.3 to 0.7. While the two wing models present

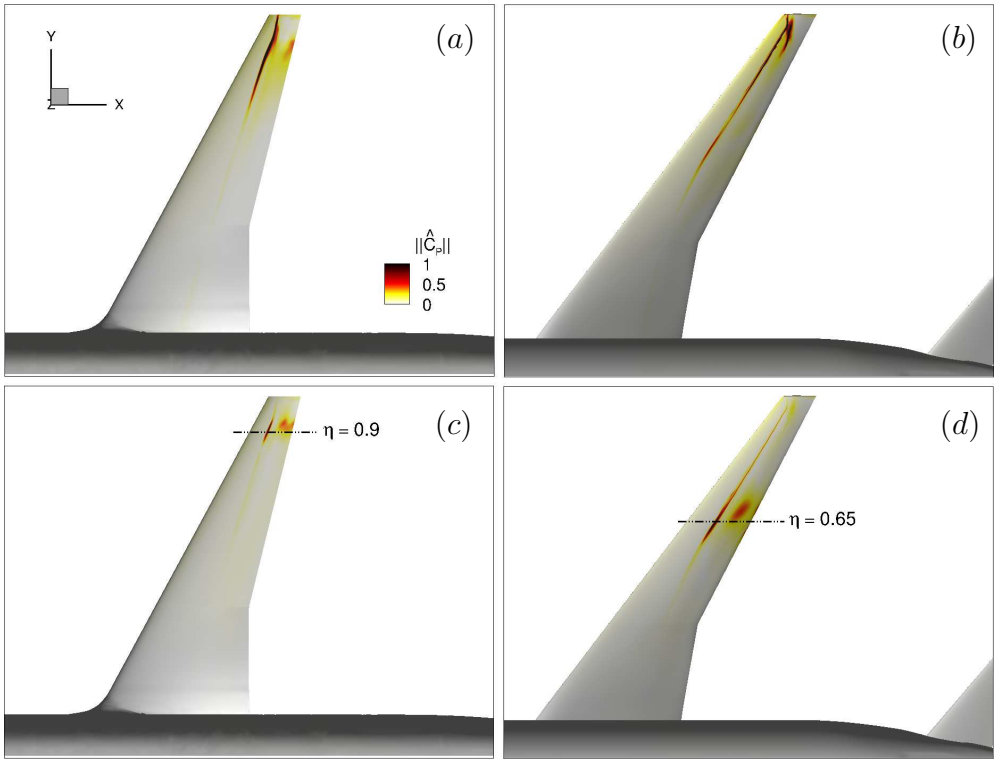

Figure 4: Magnitude of unsteady surface pressure coefficient for the RBC12 (a),(c) and CRM (b),(d). Plots of low-frequency behaviour (RBC12 $St = 0.13$, CRM $St = 0.1$) and high-frequency behaviour (RBC12 $St = 0.5$, CRM $St = 0.38$) can be found on the top and bottom, respectively. The angles of attack are $\alpha = 3°$ for the RBC12 and $\alpha = 3.6°$ for the CRM.

distinct steady states, cf. the distributed pressure loads in Figure 2, the dynamic response of the integrated loads appears to be similar, supporting the idea that a general (possibly universal) shock buffet mechanism exists. However, scrutinising the unsteady surface pressure distribution for the two wings in Figure 4, regions of high unsteady response correspond with the reverse flow in the underlying steady flow field, and hence show differences accordingly. Note again that we are considering pre-buffet conditions, where such converged and stable steady states exist. Additionally, the distributed aerodynamic response due to the forced structural excitation, as seen in Figure 4, shows spatial similarities to the self-excited shock buffet unsteadiness on the rigid wing, as seen in Figure 6. These distributed surface loads are discussed next.

Plots of the magnitude of the complex-valued unsteady surface pressure coefficient, for both the low- and high-frequency behaviours mentioned above, are presented in Figure 4. The low and high frequencies with the corresponding incidence shown in the figure are $St = 0.13$ and 0.5 at $\alpha = 3.0°$ for the RBC12 and $St = 0.09$ and 0.38 at $\alpha = 3.6°$ for the CRM. The low-frequency behaviour has not been understood entirely yet,

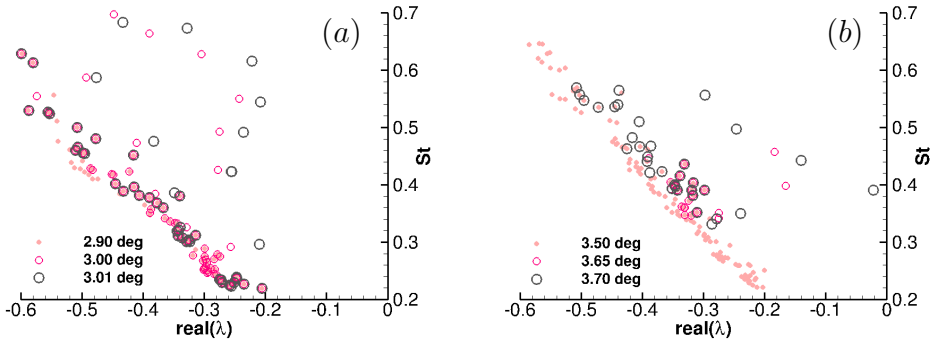

Figure 5: Eigenvalues of fluid Jacobian matrix for increasing angle of attack in the pre-buffet regime for (*a*) RBC12 and (*b*) CRM.

or at least not conclusively analysed numerically, to the authors' knowledge. From an experimental point of view, a couple of studies have shown an interesting distinct flow pattern of span-wise inboard propagation of waves along the shock front in the same lower frequency range [25,26]. Our numerical studies demonstrate that the aerodynamic response in the lower frequency range is dominated by the shock wave dynamics and this behaviour is clearly noticeable for both models. At higher frequencies, which links with the shock buffet instability, high values of shock unsteadiness are more localised with a distinct flow pattern downstream at these span locations. For the RBC12, this behaviour is located towards the wing tip region corresponding with the most-outboard region of reversed flow at around 90% of the semi-span, cf. Figure 2. For the CRM, on the other hand, this zone is shifted further inboard at about 65% semi-span, halfway between wing tip and crank. In the figure, η denotes the span-wise station non-dimensionalised by the respective semi-span length.

Figures 5 and 6 present results from the eigenmode calculations. Three-dimensional spatial structures of the amplitude function $\widehat{\boldsymbol{u}}$ are visualised for both wing cases in Figure 6, corresponding to the right-most eigenvalue in Figure 5 at $\alpha = 3.0°$ for the RBC12 and $\alpha = 3.70°$ for the CRM, respectively. The figure shows the three-dimensional mode shape of the real part of the x-momentum ($\widehat{\rho u}$) of the conservative field solution. Only the real part is shown since the imaginary part is 90° out-of-phase to allow, in this case, the span-wise outboard and stream-wise downstream propagation of the shock buffet cells. The figure also highlights how the three-dimensional buffet mode originates at the wing near the outermost station of the reverse-flow region observed in the underlying steady flow. Looking at the spatial structures and the migration of a set of eigenvalues towards the imaginary axis in Figure 5, it becomes evident that the high-frequency behaviour is linked to an absolute instability. At a critical value of a bifurcation parameter, specifically angle of attack in our study, a pair of complex-conjugate eigenvalues crosses into the unstable half-plane. In this study we restrict ourselves to the subcritical pre-buffet regime [18]. Frequencies and growth rates of the physically relevant (i.e. non-spurious) modes approaching the imaginary axis are similar near shock buffet onset for the two wing designs.

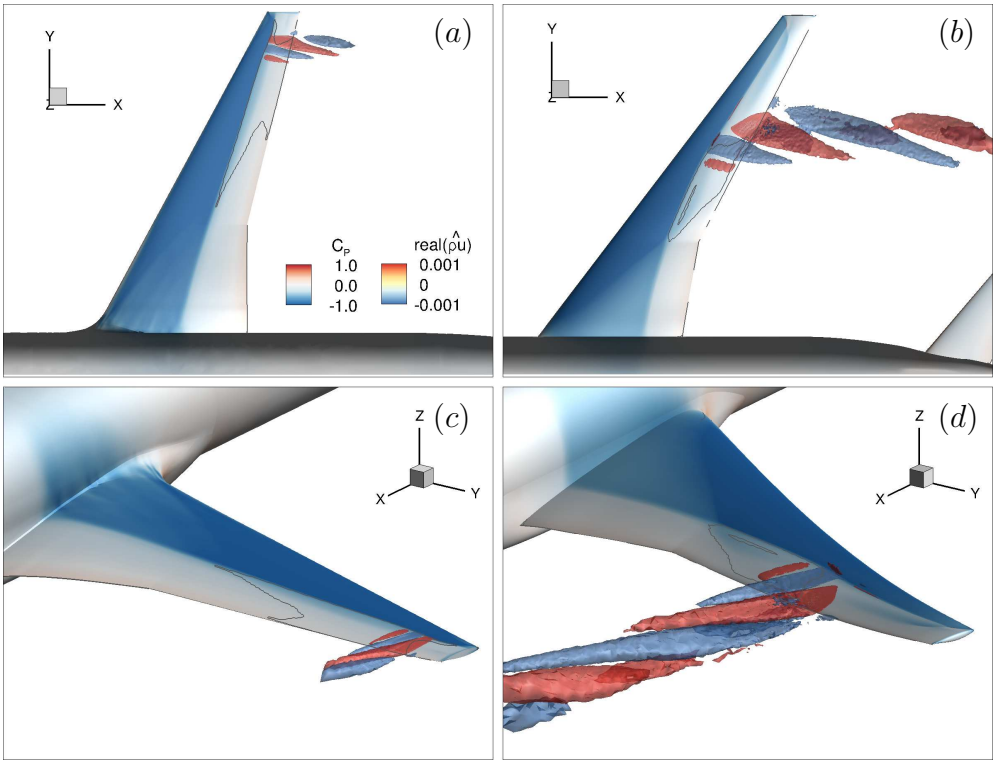

Figure 6: Spatial structure of the pre-onset three-dimensional buffet mode from global stability analysis showing iso-contour of real part of x-momentum $\widehat{\rho u}$ together with steady-state surface pressure and zero skin friction line for RBC12 at $\alpha = 3°$ (a),(c) and CRM at $\alpha = 3.7°$ (b),(d).

4.0 CONCLUSIONS

This paper presents a numerical study of the transonic edge-of-the-envelope flow over two large civil aircraft wing models. The focus is to elucidate how modern wing design improvements have affected the phenomenon of shock buffet (compared to an older-generation design) as well as to draw further conclusions on the underlying physical mechanisms of shock buffet. Time-linearised harmonic structural excitation is first discussed covering the pertinent frequency range to observe the frequency response behaviour of the integrated aerodynamic coefficients close to buffet onset. Results of the corresponding steady and unsteady distributed loads are included in the discussion, too. Finally, pre-buffet global stability results, specifically emerging distinct eigenvalues and spatial structures of right-most eigenvalues are presented briefly and linked to the insight gained from the forced excitation simulations.

Reynolds-averaged Navier–Stokes simulations reveal both similar and distinct characteristics of steady and unsteady flow features for the two wing models investigated

at their respective design Mach numbers. The modern wing design, specifically the NASA Common Research Model, demonstrates a different steady state compared to the 1970s design, referred to as RBC12, regarding the location and size of the reverse-flow region. Interestingly, the dynamic responses of integrated aerodynamic loads (such as lift coefficient) of the two models show similar trends. A low-frequency (pseudo-resonance) peak with a distinct phase lead of the aerodynamic coefficient over the structural excitation is observed that reaches its local maximum as the angle of attack is increased. For the high-frequency behaviour, the structural excitation close to the buffet onset angle of attack seems to dramatically excite an absolute instability instead. Plots of unsteady distributed loads on the other hand correspond with the differences in the steady flow fields impacting on the span-wise origin of the instability. Dynamic responses of the linearised aerodynamic coefficients for higher frequencies, in combination with the three-dimensional spatial structure of the pre-onset shock-buffet mode and the migration of eigenvalues towards the unsteady half-plane, suggest that incipient shock buffet on wings can be treated as a linear stability problem.

For future work, a link between the low-frequency behaviour, which to date has not been fully explained or understood, and a possible additional instability mechanism should be looked into further. Different forms of excitation, other than harmonic structural forcing, would allow to better comprehend the underlying mechanisms of shock buffet. Finally, interesting results could come out from reiterating the modern-wing simulations, this time without taking into account static deformation to scrutinise the effects of structural deformation on shock-buffet behaviour. In the long-term, fully-coupled fluid-structure simulation is required considering the inherent multidisciplinary nature of edge-of-the-envelope flight physics.

ACKNOWLEDGEMENTS

The authors wish to acknowledge Airbus Group for sponsoring the PhD studentship. We also wish to thank Aircraft Research Association for making the RBC12 model available for this study.

REFERENCES

1. EASA, "CS25 - Certification Specifications for Large Aeroplanes," 2009.
2. W. F. Hilton and R. G. Fowler, *Photographs of shock wave movement*. HM Stationery Office, 1952.
3. B. Lee, "Oscillatory shock motion caused by transonic shock boundary-layer interaction," *AIAA Journal*, vol. 28, no. 5, pp. 942–944, 1990.
4. J. Crouch, A. Garbaruk, D. Magidov, and A. Travin, "Origin of transonic buffet on aerofoils," *Journal of Fluid Mechanics*, vol. 628, pp. 357–369, 2009.
5. J. Crouch, A. Garbaruk, and D. Magidov, "Predicting the onset of flow unsteadiness based on global instability," *Journal of Computational Physics*, vol. 224, no. 2, pp. 924–940, 2007.
6. B. Lee, "Self-sustained shock oscillations on airfoils at transonic speeds," *Progress in Aerospace Sciences*, vol. 37, no. 2, pp. 147–196, 2001.

7. L. Jacquin, P. Molton, S. Deck, B. Maury, and D. Soulevant, "Experimental study of shock oscillation over a transonic supercritical profile," *AIAA Journal*, vol. 47, no. 9, pp. 1985–1994, 2009.
8. B. Benoit and I. Legrain, "Buffeting prediction for transport aircraft applications based on unsteady pressure measurements," in *5th Applied Aerodynamics Conference*, 1987. AIAA 1987-2356.
9. F. Roos, "The buffeting pressure field of a high-aspect-ratio swept wing," in *18th Fluid Dynamics and Plasmadynamics and Lasers Conference*, 1985. AIAA 1985-1609.
10. M. Iovnovich and D. E. Raveh, "Numerical study of shock buffet on three-dimensional wings," *AIAA Journal*, vol. 53, no. 2, pp. 449–463, 2015.
11. S. Lawson, D. Greenwell, and M. K. Quinn, "Characterisation of buffet on a civil aircraft wing," in *54th AIAA Aerospace Sciences Meeting*, 2016. AIAA 2016-1309.
12. S. Koike, M. Ueno, K. Nakakita, and A. Hashimoto, "Unsteady pressure measurement of transonic buffet on NASA Common Research Model," in *34th AIAA Applied Aerodynamics Conference*, 2016. AIAA 2016-4044.
13. N. Giannelis, G. Vio, and O. Levinski, "A review of recent developments in the understanding of transonic shock buffet," *Progress in Aerospace Sciences*, vol. 92, pp. 39–84, 2017.
14. V. Brunet and S. Deck, "Zonal-detached eddy simulation of transonic buffet on a civil aircraft type configuration," in *38th Fluid Dynamics Conference and Exhibit, Fluid Dynamics and Co-located Conferences*, 2008. AIAA 2008–4152.
15. F. Sartor and S. Timme, "Reynolds-averaged Navier–Stokes simulations of shock buffet on half wing-body configuration," in *53rd AIAA Aerospace Sciences Meeting*, 2015. AIAA 2015–1939.
16. F. Sartor and S. Timme, "Delayed detached-eddy simulation of shock buffet on half wing-body configuration," *AIAA Journal*, vol. 55, no. 4, pp. 1230–1240, 2017.
17. S. Timme and R. Thormann, "Towards three-dimensional global stability analysis of transonic shock buffet," in *AIAA Atmospheric Flight Mechanics Conference*, 2016. AIAA 2016-3848.
18. S. Timme, "Global instability of wing shock buffet," *arXiv e-prints*, 2018. arXiv:1806.07299 [physics.flu-dyn].
19. J. Vassberg, M. Dehaan, M. Rivers, and R. Wahls, "Development of a Common Research Model for applied CFD validation studies," in *26th AIAA Applied Aerodynamics Conference*, 2008. AIAA 2008-6919.
20. S. Xu, S. Timme, and K. J. Badcock, "Enabling off-design linearised aerodynamics analysis using Krylov subspace recycling technique," *Computers & Fluids*, vol. 140, pp. 385–396, 2016.
21. R. Thormann and M. Widhalm, "Linear-frequency-domain predictions of dynamic-response data for viscous transonic flows," *AIAA Journal*, vol. 51, no. 11, pp. 2540–2557, 2013.

22. D. C. Sorensen, "Implicit application of polynomial filters in a k-step arnoldi method," *SIAM Journal on Matrix Analysis and Applications*, vol. 13, no. 1, pp. 357–385, 1992.

23. R. Lehoucq, D. Sorensen, and C. Yang, *ARPACK Users' Guide*. SIAM, 1998.

24. J. Nitzsche, "A numerical study on aerodynamic resonance in transonic separated flow," in *International Forum on Aeroelasticity and Structural Dynamics (IFASD), Seattle, USA*, 2009. IFASD-2009-126.

25. J. Dandois, "Experimental study of transonic buffet phenomenon on a 3D swept wing," *Physics of Fluids*, vol. 28, no. 1, p. 016101, 2016.

26. L. Masini, S. Timme, A. Ciarella, and A. Peace, "Influence of vane vortex generators on transonic wing buffet: further analysis of the BUCOLIC experimental dataset," in *Proceedings of the 52nd 3AF International Conference on Applied Aerodynamics, Lyon, France (2017)*, 2017.